NANO LETTERS

2005
Vol. 5, No. 11
2257−2261

Electroluminescence from a Single-Nanocrystal Transistor

Mark S. Gudiksen,[†] Kristin N. Maher,[†] Lian Ouyang,[†] and Hongkun Park*[,†,‡]

Department of Chemistry and Chemical Biology, and Department of Physics, Harvard University, Cambridge, Massachusetts 02138

Received August 12, 2005; Revised Manuscript Received September 8, 2005

ABSTRACT

We report the fabrication and characterization of light-emitting transistors incorporating individual cadmium selenide (CdSe) nanocrystals. Electrical measurements conducted at low bias voltage and low temperature show clear evidence of Coulomb blockade behavior, indicating that electrons pass through the nanocrystal by single-electron tunneling. Once the bias voltage exceeds the band gap of CdSe, devices with asymmetric tunnel barriers emit linearly polarized light. Combined analyses of the electrical and optical data indicate that the tunnel couplings between the nanorod and the metallic electrodes change significantly as a function of bias voltage and light emission results from the inelastic scattering of tunneling electrons.

Semiconductor nanocrystals have emerged as promising materials for optoelectronic applications[1−6] because they exhibit electrical and optical properties that vary significantly with their size, while possessing solution-phase processibility akin to organic materials. A variety of optoelectronic devices based on nanocrystal ensembles have been realized already by exploiting these properties, including photovoltaic cells,[2] light-emitting diodes,[3,4] and optically pumped lasers.[5,6]

Physical investigations of individual nanocrystals[7−9] have received considerable attention from the scientific community because a single nanocrystal represents the miniaturization limit of ensemble-based devices. These studies also allow the detailed interrogation of nanocrystal properties without the complications of ensemble averaging. Electrically driven light-emitting devices based on individual nanocrystals have not been realized to date, however, and the interplay between charge transport and photon emission within a single nanocrystal has not been investigated in detail.

Here we report the fabrication and characterization of light-emitting transistors incorporating individual CdSe nanocrystals. Unlike the two-terminal devices employed in most previous studies of nanoscale light emitters,[10−17] three-terminal transistors enable a detailed characterization of the electron transport and light emission mechanisms of individual nanocrystals while systematically varying their electrostatic potential. Specifically, simultaneous measurements of the electrical and optical behavior of single-nanocrystal transistors reveal that the voltage-dependent variation of nanocrystal−metal junctions plays a crucial role in the light-emission process, and electroluminescence (EL) from a single-nanocrystal transistor results from resonantly enhanced inelastic scattering of tunneling electrons,[15−18] a mechanism that has not been invoked previously in nanocrystal-based devices.

Single-nanocrystal transistors (SNCTs) were fabricated by first synthesizing rod-shaped CdSe nanocrystals (CdSe nanorods) using a solution-based approach.[19,20] The nanorods were then deposited from solution onto a degenerately doped silicon wafer coated with 300-nm thick oxide, and individual, isolated nanorods were located with respect to predefined alignment marks. Source and drain electrodes contacting individual nanorods were defined using electron-beam lithography, and the doped silicon substrate was used as a gate electrode. A representative scanning electron micrograph of a resulting device is presented in Figure 1a, showing a single nanorod contacted by two gold electrodes with ∼30 nm separation.

Measurements of SNCTs were performed in a cryostat coupled with an optical microscope at low temperature (∼10 K). EL data were collected using an intensified charge-coupled device (CCD) camera or an avalanche photodiode, and spectroscopic measurements were performed by dispersing the nanorod emission onto the CCD with a grating. Figure 1c shows representative current−voltage and EL data collected from a device, **D1**. The device exhibits a low-bias conductance gap followed by a nonlinear increase in current (I) at high bias voltage (V). Concomitant measurements of EL intensity show that the device begins to emit light once V reaches a threshold (V_{th}) of ±1.7 V (±0.1 V) independent of bias polarity. Similar optoelectronic behavior was observed for more than 20 nanorod devices measured to date.

* To whom correspondence should be addressed. E-mail: Hongkun_Park@harvard.edu.
[†] Department of Chemistry and Chemical Biology.
[‡] Department of Physics.

10.1021/nl0516005 CCC: $30.25
Published on Web 10/01/2005

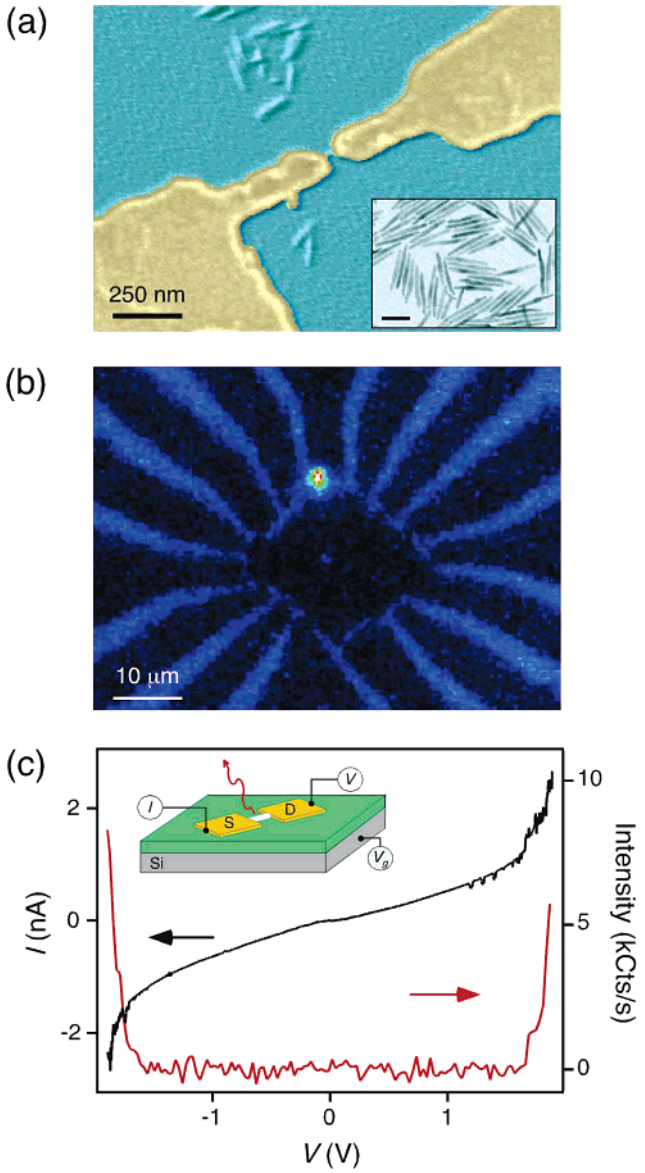

Figure 1. (a) Scanning electron microscope image (false color) of a CdSe-nanorod transistor. The inset shows a transmission electron microscope image of the as-synthesized CdSe nanorods (scale bar is 50 nm). (b) Optical microscope image showing electroluminescence (EL) from a nanorod transistor. (c) Current (I) (black) and simultaneously measured EL intensity (red) plotted against bias voltage (V) obtained from device **D1**. The inset gives a schematic illustration of the transistor geometry, showing source (S) and drain (D) electrodes contacting the nanorod with a back gate.

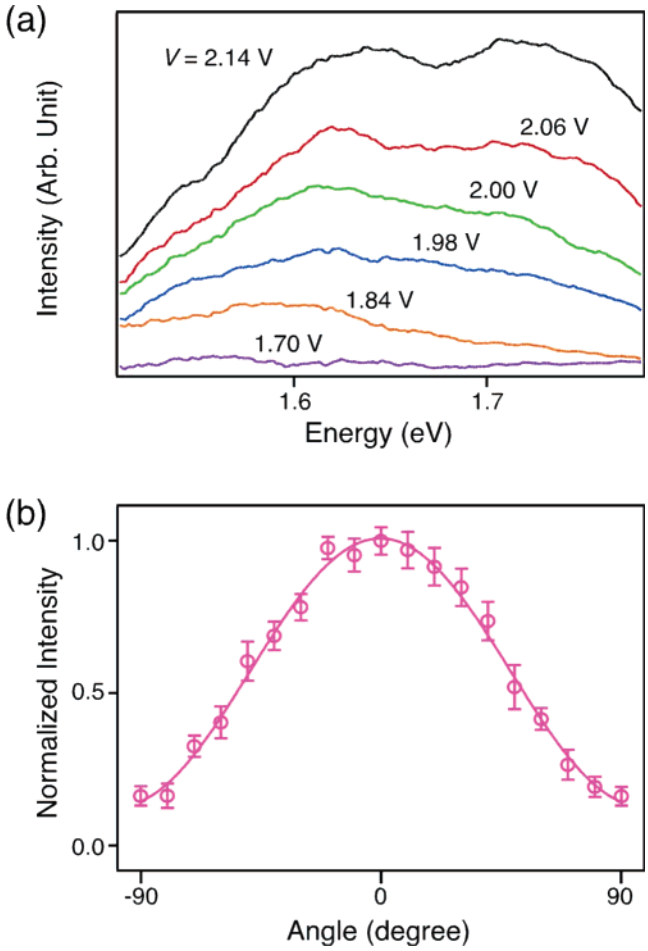

Figure 2. (a) EL spectra of device **D2** at different bias voltages. The threshold voltage, V_{th}, at which **D2** started to emit light was 1.75 (±0.05) V. (b) Normalized EL intensity as a function of polarizer angle with respect to the nanorod axis (error bars represent 1σ). The solid line is a $\cos^2\theta$ fit to the data, providing the polarization value, P, for this device of 0.77.

The photon-counting measurements, such as those shown in Figure 1c, show that a typical number of detected photons is 10^3-10^4 s^{-1} when the current flowing through the device is 1−10 nA. Given that the photon collection efficiency of our experimental setup is on the order of 1%, the observed photon count indicates that the EL efficiency of a SNCT corresponds to $\sim10^{-5}$ photons per electron passage. This value is approximately 2 orders of magnitude smaller than the best EL efficiency reported from a nanocrystal-organic hybrid light-emitting diode.[4]

Figure 2a displays EL spectra obtained from another device, **D2**, at different V. When V exceeded 2.2 V, the device became unstable, eventually resulting in device failure. The spectra in Figure 2a demonstrate that the energies of emitted photons always exceed eV_{th} and extend up to eV (see the Supporting Information). They also show two peaks at energies of ∼1.65 eV and ∼1.72 eV superposed on the broad background. Comparison with ensemble photoluminescence (PL) spectra indicates that the 1.72-eV feature corresponds to band-gap emission from a CdSe nanorod, confirming that EL originates from the nanorod. The lower energy peak at ∼1.65 eV is assigned to emission from surface states, in accordance with previous PL[21] and chemiluminescence experiments.[22] The prominent appearance of surface emission is most likely due to the loss of surface-capping ligands during the device-fabrication process.

The photons emitted from a SNCT are highly polarized along the nanorod axis, as shown in Figure 2b. The degree of linear polarization can be quantified by calculating the polarization values, P, defined as $(I_{||} - I_{\perp})/(I_{||} + I_{\perp})$. Here $I_{||}$ and $I_{\perp}$ are the light intensities parallel and perpendicular to the nanorod axis, respectively. Fitting of the polarization data from several devices yields an average P of 0.7 ± 0.1, in excellent agreement with the PL measurements on individual

nanorods.[8] The observed polarized emission can result from two distinct mechanisms: the dielectric contrast of the nanorod with respect to its surroundings[23,24] and the unique electronic structure of CdSe.[8] A simple estimate based on the dielectric contrast mechanism, which treats the nanorod as an ellipsoid with an aspect ratio of 3:1 and uses an average dielectric constant of 2.5 for the surroundings, yields a P value of ~0.5. This estimate indicates that although the dielectric contrast mechanism accounts for the bulk of the observed P, the band structure of CdSe should also be invoked to explain P values fully.[8]

Further insight into the EL can be obtained by analyzing the $I-V$ characteristics of light-emitting SNCTs in detail. As exemplified in Figure 1, these devices generally exhibited a low-bias zero-conductance region followed by nonlinear increase in current at higher bias. Some devices exhibited a conductance gap extending over $V > 0.5$ V, whereas other devices exhibited a much smaller conductance gap that could be reduced to zero by adjusting V_g (see the Supporting Information). The observation of these two types of behavior indicates that the alignment between the metal Fermi level and the CdSe band gap varies from device to device, depending on the local electrostatic environment.

Figure 3a shows a plot of differential conductance (dI/dV) as a function of V and gate voltage (V_g) obtained from a representative device, **D3**, with a small conductance gap. Two distinct features are observed in the $dI/dV-V-V_g$ plot: diamond-shaped zero-conductance regions near zero bias and a series of conductance peaks that vary linearly with V_g. Both of these features are classic signatures of Coulomb blockade behavior, and indicate that the electrons pass through the device via single-electron tunneling.[9,25]

The prominent appearance of dI/dV peaks with only one slope in Figure 3a indicates that the tunnel couplings between the nanorod and two electrodes are highly asymmetric. A quantitative estimate of this asymmetric coupling can be obtained by fitting the transport data using a Coulomb blockade model[25] and by extracting the tunnel resistance values, R_s and R_d, for the source and drain electrodes. For the device shown in Figure 3a, R_s and R_d are found to be 0.4 GΩ and 4.6 GΩ near zero bias. Significantly, all of the light-emitting devices exhibited asymmetric tunnel couplings, whereas devices with symmetric couplings emitted little or no light.

The $I-V$ characteristics at high V provide insight into the nature of the tunnel barriers. The orthodox Coulomb blockade model typically assumes that the tunnel couplings between the nanorod and electrodes are independent of V, and thus the device behavior converges to ohmic (linear) transport at high bias. As shown in Figure 1c, our nanorod devices display superlinear $I-V$ behavior at high V, however, suggesting that the tunnel resistances, R_s and R_d, vary with V.

Figure 3b shows a comparison of the $dI/dV-V$ data with the result of a model fit where the V dependence of R_s and R_d is included explicitly. This figure demonstrates that the variable resistance model accounts for the experimental data extremely well. The inset of Figure 3b, which plots R_s and

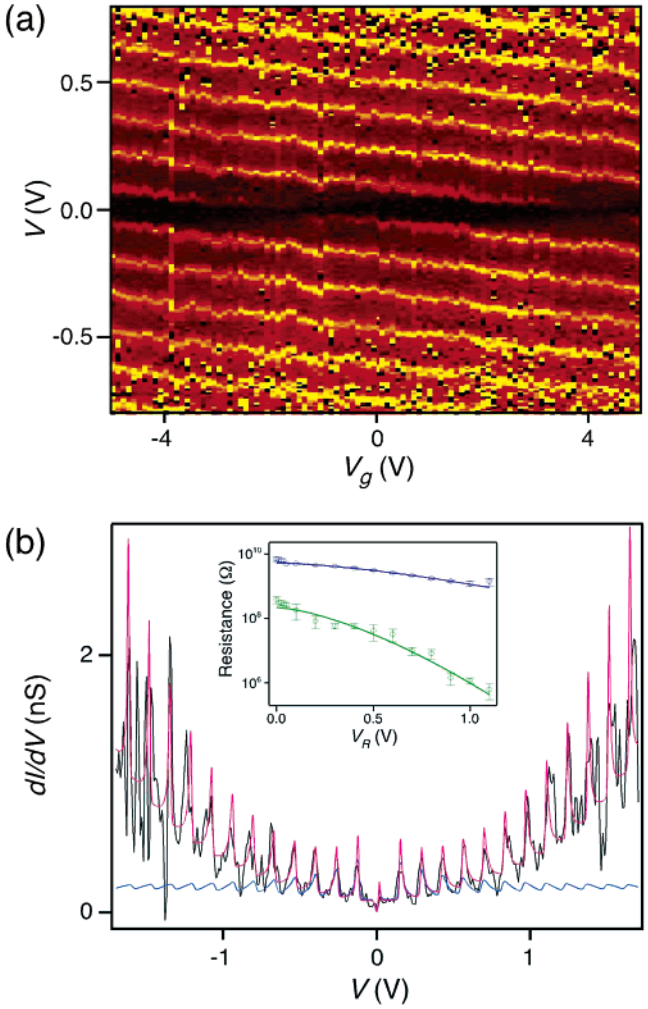

Figure 3. (a) Plot of differential conductance (dI/dV) as a function of V and gate voltage (V_g) of device **D3**. The dI/dV values are represented by a color scale from dark red (0) to bright yellow (1 nS). Analysis of the data using a Coulomb blockade model yields source, drain, and gate capacitances of $C_s = 1.1$ aF, $C_d = 1.2$ aF, and $C_g = 0.029$ aF, respectively. The source and drain tunnel resistance values near zero bias are determined to be $R_s = 0.4$ GΩ and $R_d = 4.6$ GΩ. (b) Comparison of experimental dI/dV (black) and calculated dI/dV values from constant (blue) and variable resistance (red) models as a function of V. The inset shows R_s (green) and R_d (blue) obtained from the variable resistance fit versus the voltage drop, V_R, at each junction (error bars represent 1σ). The functions used for the variable resistance model were given by $R_s(V_{Rs}) = 0.22 \exp(-5.4\ V_{Rs}^{3/2})$ GΩ and $R_d(V_{Rd}) = 5.3 \exp(-1.5\ V_{Rd}^{3/2})$ GΩ. The voltage drop across each junction is given by $V_{Rs(d)} = (C_{d(s)}/(C_s + C_d))V$.

R_d from the fit against the voltage drop (V_R) at each barrier, further indicates that both resistances decrease with increasing V_R. The observed V dependence follows the form $R_{s,d}(V_R) \propto \exp(-V_R^{-3/2})$, consistent with tunneling through a triangular barrier.[26] Significantly, the result in the Figure 3b inset indicates that when the bias voltage reaches the EL threshold the smaller tunnel resistance effectively vanishes, and thus the transport through the device becomes single-barrier tunneling.

In principle, the EL from individual nanorods can result from several mechanisms, including the resonant injection of electrons and holes into the nanorod[26,27] and the inelastic

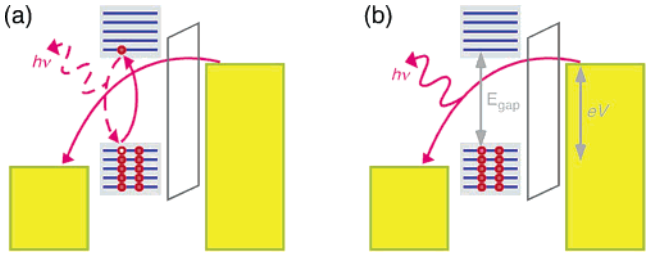

Figure 4. Mechanism for nanorod EL. Photons can be emitted (a) when the electron−hole pairs excited by inelastic scattering of tunneling electrons recombine or (b) directly from electrons that tunnel inelastically through the barrier.

scattering of tunneling electrons.[15−18] The electrical and optical data presented in Figures 1−3 place stringent constraints on these models, however, and allow for the discrimination between different scenarios. Specifically, the device behavior at low bias indicates that alignment between the metal Fermi levels and the CdSe band gap varies from device to device.[4,9] Irrespective of this initial alignment, however, devices with asymmetric tunnel couplings emit linearly polarized light when $|V|$ exceeds $|V_{th}|$ in either positive or negative bias, and electrons (or holes) pass through the device via single-barrier tunneling. Finally, the value of eV_{th} is always close to the nanorod band gap.

Taken together, these observations suggest that the resonant electron/hole injection mechanism traditionally invoked for semiconductor light sources[26,27] is not applicable to our devices. In this scenario, electron−hole pairs are injected into the nanorod as the Fermi level of one electrode aligns with the conduction band while the other aligns with the valence band. Our transport data, such as that as shown in Figure 3, indicate, however, that the capacitive couplings to source and drain electrodes are nearly equal in our devices, and thus the Fermi level shifts in each electrode as a function of V should be given by $\sim V/2$. Within the framework of the resonant charge injection model, eV_{th} in device **D3** should then be approximately twice the band gap because the Fermi levels at zero bias lie near one of the bands. This prediction clearly contradicts our observation that eV_{th} is always close to the nanorod band gap irrespective of the size of the zero conductance region.

The data in Figures 1−3 instead indicate that the EL in our devices can be best explained by inelastic scattering of tunneling electrons.[15−18] As shown in Figure 3b, the electrons pass through the device via essentially single-barrier tunneling near the onset of EL because of the rapid decrease of the smaller tunnel resistance caused by the increase in bias voltage. When $e|V|$ exceeds the band gap of the nanorod, the electrons tunneling through the barrier have sufficient energy to scatter inelastically and excite an electron−hole pair within the nanorod, which then recombines to emit light (Figure 4a). Alternatively, the EL can result directly from inelastically tunneling electrons (akin to Bremsstrahlung[28]), the efficiency of which is resonantly enhanced when eV matches the band gap (Figure 4b). We note that these two scenarios are equivalent in the limit of instantaneous electron−hole recombination.

The spectral features observed in Figure 2 are fully consistent with this inelastic scattering mechanism. Within this mechanism, the energy of emitted photons should range between the CdSe band gap and eV irrespective of bias polarity because the only energetic constraint is provided by the energy of tunneling electrons. Moreover, the large width of spectral features in Figure 2a is a direct consequence of the short time scale associated with this inelastic scattering process. Finally, the relatively low EL efficiency ($\sim 10^{-5}$) observed in our devices is consistent with the low efficiency of the inelastic tunneling process.

The present experiments demonstrate that the three-terminal transistor geometry provides a powerful platform for studying the interplay between charge transport and light emission in chemically derived nanostructures. This approach can be extended to other systems, such as nanorod heterostructures[11,29,30] and single-molecule devices,[31−33] and should also enable the exploration of other possibilities, such as electrically driven single photon sources[27,34] and spin-injection devices.[35]

Acknowledgment. We acknowledge Mandar Deshmukh for helpful discussions. This work was supported by NSF, ARO, the Packard Foundation, and DARPA.

Supporting Information Available: $I-V$ curves in Figure S1 illustrate two types of electrical behavior exhibited by SNCTs. Spectra in Figure S2 show electroluminescense peak shapes at higher energies as a function of bias voltage. This material is available free of charge via the Internet at http://pubs.acs.org.

References

(1) Alivisatos, A. P. *Science* **1996**, *271*, 933.
(2) Huynh, W. U.; Dittmer, J. J.; Alivisatos, A. P. *Science* **2002**, *295*, 2425.
(3) Colvin, V. L.; Schlamp, M. C.; Alivisatos, A. P. *Nature* **1994**, *370*, 354.
(4) Coe, S.; Woo, W.-K.; Bawendi, M.; Bulovic, V. *Nature* **2002**, *420*, 800.
(5) Klimov, V. I.; Mikhailovsky, A. A.; Xu, S.; Malko, A.; Hollingsworth, J. A.; Leatherdale, C. A.; Eisler, H.-J.; Bawendi, M. G. *Science* **2000**, *290*, 314.
(6) Kazes, M.; Lewis, D. Y.; Ebenstein, Y.; Mokari, T.; Banin, U. *Adv. Mater.* **2002**, *14*, 317.
(7) Nirmal, M.; Brus, L. *Acc. Chem. Res.* **1999**, *32*, 407.
(8) Hu, J. T.; Li, L. S.; Yang, W. D.; Manna, L.; Wang, L. W.; Alivisatos, A. P. *Science* **2001**, *292*, 2060.
(9) Klein, D. L.; Roth, R.; Lim, A. K. L.; Alivisatos, A. P.; McEuen, P. L. *Nature* **1997**, *389*, 699.
(10) Duan, X.; Huang, Y.; Cui, Y.; Wang, J.; Lieber, C. M. *Nature* **2001**, *409*, 66.
(11) Gudiksen, M. S.; Lauhon, L. J.; Wang, J.; Smith, D. C.; Lieber, C. M. *Nature* **2002**, *415*, 617.
(12) Lee, T. H.; Gonzalez, J. I.; Dickson, R. M. *Proc. Natl. Acad. Sci.* **2002**, *99*, 10272.
(13) Baier, M. H.; Constantin, C.; Pelucchi, E.; Kapon, E. *Appl. Phys. Lett.* **2004**, *84*, 1967.
(14) Misewich, J. A.; Martel, R.; Avouris, P.; Tsang, J. C.; Heinze, S.; Tersoff, J. *Science* **2003**, *300*, 783.
(15) Berndt, R.; Gaisch, R.; Gimzewski, J. K.; Reihl, B.; Schittler, R. R.; Schneider, W. D.; Tschudy, M. *Science* **1993**, *262*, 1425.
(16) Qiu, X. H.; Nazin, G. V.; Ho, W. *Science* **2003**, *299*, 542.
(17) Nazin, G. V.; Qiu, X. H.; Ho, W. *Phys. Rev. Lett.* **2003**, *90*, 216110.
(18) Khanna, S. K.; Lambe, J. *Science* **1983**, *220*, 1345.
(19) Peng, X. G.; Manna, L.; Yang, W.; Wickham, J.; Scher, E.; Kadavanich, A.; Alivisatos, A. P. *Nature* **2000**, *404*, 59.

(20) Peng, Z. A.; Peng, X. G. *J. Am. Chem. Soc.* **2002**, *124*, 3343.
(21) Hines, M. A.; Guyot-Sionnest, P. *J. Phys. Chem.* **1996**, *100*, 468.
(22) Myung, N.; Ding, Z. F.; Bard, A. J. *Nano Lett.* **2002**, *2*, 1315.
(23) Wang, J. F.; Gudiksen, M. S.; Duan, X. F.; Cui, Y.; Lieber, C. M. *Science* **2001**, *293*, 1455.
(24) Kovalev, D.; Ben Chorin, M.; Diener, J.; Koch, F.; Efros, A. L.; Rosen, M.; Gipppius, N. A.; Tikhodeev, S. G. *Appl. Phys. Lett.* **1995**, *67*, 1585.
(25) Grabert, H.; Devoret, M. H. *Single Charge Tunneling*; Plenum: New York, 1992.
(26) Sze, S. M. *Physics of Semiconductor Devices*; Wiley-Interscience: New York, 1981.
(27) Kim, J.; Benson, O.; Kan, H.; Yamamoto, Y. *Nature* **1999**, *397*, 500.
(28) Cohen-Tannoudji, C.; Dupont-Roc, J.; Grynberg, G. *Atom-Photon Interactions: Basic Processes and* Applications; John Wiley & Sons: New York, 1992.
(29) Milliron, D. J.; Hughes, S. M.; Cui, Y.; Manna, L.; Li, J.; Wang, L.-W.; Alivisatos, A. P. *Nature* **2004**, *430*, 190.
(30) Mokari, T.; Rothenberg, E.; Popov, I.; Costi, R.; Banin, U. *Science* **2004**, *304*, 1787.
(31) Park, H.; Park, J.; Lim, A. K. L.; Anderson, E. H.; Alivisatos, A. P.; McEuen, P. L. *Nature* **2000**, *407*, 57.
(32) Liang, W. J.; Shores, M. P.; Bockrath, M.; Long, J. R.; Park, H. *Nature* **2002**, *417*, 725.
(33) Park, J.; Pasupathy, A. N.; Goldsmith, J. I.; Chang, C.; Yaish, Y.; Petta, J. R.; Rinkoski, M.; Sethna, J. P.; Abruña, H. D.; McEuen, P. L.; Ralph, D. C. *Nature* **2002**, *417*, 722.
(34) Yuan, Z. L.; Kardynal, B. E.; Stevenson, R. M.; Shields, A. J.; Lobo, C. J.; Cooper, K.; Beattie, N. S.; Ritchie, D. A.; Pepper, M. *Science* **2002**, *295*, 102.
(35) Fiederling, R.; Keim, M.; Reuscher, G.; Ossau, W.; Schmidt, G.; Waag, A.; Molenkamp, L. W. *Nature* **1999**, *402*, 787.

NL0516005